Available online at www.sciencedirect.com
ScienceDirect
Journal of Sound and Vibration 316 (2008) 1–24
JOURNAL OF SOUND AND VIBRATION
www.elsevier.com/locate/jsvi

Review

Modeling of coupled structural systems by an energy spectral element method

E.R.O. Santos*, J.R.F. Arruda, J.M.C. Dos Santos

Department of Computational Mechanics, Faculty of Mechanical Engineering, State University of Campinas, C. Postal 6122, Campinas 13083-970, SP, Brazil

Received 29 June 2006; received in revised form 11 February 2008; accepted 18 February 2008
Handling Editor S. Bolton
Available online 9 April 2008

Abstract

Solving approximate energy flow partial differential equations for structural elements can be done analytically (energy flow analysis—EFA) or using finite element approximations (energy finite element method—EFEM). In this paper, energy equations are solved using the spectral element method (SEM). This new approach, which is called the energy spectral element method (ESEM), can be applied to predict the distribution of the energy flow and energy density of built-up structures at high frequencies. Energy spectral element method is a matrix formulation based on the general solution of the partial differential equations for energy density in structural vibrations such as longitudinal and transversal vibrations of frames. A spectral energy element can be shown to be equivalent to an infinite number of energy finite elements. In this work, numerical models involving coupled rods and beams are generated by energy spectral element method, and the results obtained are compared with energy densities computed from the displacement fields predicted by the SEM to solve the conventional boundary value problem.

Contents

*Corresponding author. Tel.: +55 11 33790285.
E-mail addresses: oliveira@fem.unicamp.br (E.R.O. Santos), arruda@fem.unicamp.br (J.R.F. Arruda), zema@fem.unicamp.br (J.M.C. Dos Santos).

0022-460X/$ - see front matter © 2008 Elsevier Ltd. All rights reserved.
doi:10.1016/j.jsv.2008.02.039

1. Introduction

Acoustic and vibrational energies are frequently borne by waveguides such as rods and beams. Many built-up structures include this type of component, which acts as an important vibration and noise transmission path. A review of the literature indicates that although structural dynamic analysis at low frequency has been developed extensively, there is a demand for predictive tools able to solve this problem in mid- and high-frequency ranges. Traditional numerical methods such as the finite element method (FEM) and the boundary element method (BEM) have been used to solve structural dynamic problems. However, in complex systems, they have an inherent characteristic that generates large model sizes at high frequencies. Therefore, the mid- and high-frequency behavior of structures is still an active subject of investigation.

A vast amount of research has been dedicated to the high-frequency range, and one of the techniques most commonly used is statistical energy analysis (SEA), which was first presented in the early 1960s [1]. In SEA, the structure is divided into a set of subsystems that interact through the exchange of energy. SEA is aimed at predicting the vibrational energy level in each subsystem. Once computed, these energies can be used to estimate acceleration and stress levels in the subsystems. However, the spatial variation of the response within each subsystem cannot be obtained, since SEA provides one energy level for each subsystem. For purposes of design at high frequencies, it would be useful to know the spatial vibrational behavior of the entire structure.

Based on the analogy between mechanical energy flow and thermal energy flow, Wohlever and Bernhard [2] proposed the energy flow analysis (EFA). This is an approximated analytical energy solution for rods and beams which requires much fewer parameters and less computational effort than that required to model the exact analytical energy solution using displacement formulations. The governing equations of EFA use the proportionality relationship between power flow (intensity) and the gradient of the energy density by establishing an energy balance on a differential control volume. Cho and Bernhard [3] used EFA governing equations and coupling relationships to predict the spatial and frequency-averaged vibrational response of frame structures. Coupling relationships were used to describe the energy transfer for different types of joints, such as beam–beam, rod–beam, plate–plate, and structure–acoustic cavity coupling. This approach was also extended by Bouthier and Bernhard to membranes [4] and plates [5], and by Bitsie and Bernhard to vibroacoustic problems [6]. All these studies used analytical and finite element approximation solutions of partial energy differential equations to predict spatial and frequency-averaged vibration behavior in order to identify how vibrations propagate through a built-up structure at high frequencies.

Developed by Doyle [7], the spectral element method (SEM) is the frequency domain exact analytical solution of the wave equation, using displacement formulation, tailored with the matrix ideas of the FEM. In this method, built-up structures with geometrically uniform members can be represented with a single spectral beam element, significantly reducing the total number of degrees of freedom compared with other methods. It can be shown that one spectral element is equivalent to an infinite number of finite elements [7]. In addition, the wave propagation in the members is accurately expressed because the exact solution of rods and beams in the frequency domain is obtained. However, there are still difficulties to model nonuniform members and to apply arbitrary boundary conditions.

This paper presents a new application of the SEM, which was originally proposed by Santos [8] and called energy spectral element method (ESEM). It consists basically in applying the same matrix methodology of the spectral element to the EFA governing equations for rods and beams. Similarly to EFA, the ESEM requires a joint element [3] to connect two or more structural elements, while in SEM this is already included in the formulation. Compared to similar displacement formulations, it has the advantage of modeling only energy variations and, since energy variations are smoother than displacement variations, it is efficient over a large frequency range. It is also able to calculate high-frequency energy density for the entire space domain of the structural member with the same accuracy, provided there is enough modal density in the frequency band of

interest [9]. Therefore, the method can address the high-frequency range, where displacement methods are too expensive and the SEA solution does not yield the spatial behavior with sufficient detail. The results obtained by the proposed method are verified using the energy density computed from the exact analytical solution of the wave equation obtained by using a displacement SEM formulation.

The examples treated in this paper use the elementary rod theory and the Bernoulli–Euler beam theory to formulate a spectral frame element for the planar vibration problem. The main differences between the results obtained with SEM and ESEM stem from the validity limits of ESEM formulation and coupling relationships in the frequency band of interest.

2. Spectral element method

The SEM is a matrix methodology similar to the FEM for handling structural wave propagation problems. The frequency domain dynamic stiffness relation for the spectral element is established via dynamic shape functions between element nodes, which are the exact displacement distributions of the theory considered.

In this paper, the fundamental equation is derived for a longitudinal wave in a rod. Fig. 1 shows an elastic two-noded rod element with a uniform cross-section subjected to dynamic forces at both ends. Considering that rod deformation depends on the undamped elementary rod theory, an equilibrium equation and boundary conditions at both ends are obtained as

$$ES\frac{\mathrm{d}^2u}{\mathrm{d}x^2}-\rho S\frac{\mathrm{d}^2u}{\mathrm{d}t^2}=0, \tag{1}$$

$$ES\left(\frac{\mathrm{d}u}{\mathrm{d}x}\right)_1=F_1, \quad ES\left(\frac{\mathrm{d}u}{\mathrm{d}x}\right)_2=F_2, \tag{2}$$

where E, S, and ρ are Young's modulus, the cross-section area, and the mass density, respectively; u is the longitudinal displacement, which is a function of the spatial coordinate x and time t; F_1 and F_2 are the external axial forces; and subscripts 1 and 2 denote values at the element rod node numbers 1 and 2, respectively.

By applying the Fourier transform to both sides of Eq. (1), its spectral representation can be written as

$$ES\frac{\mathrm{d}^2\widehat{u}}{\mathrm{d}x^2}+\omega^2\rho S\widehat{u}=0, \tag{3}$$

where $\widehat{\ }$ denotes that the function is Fourier transformed and ω is the circular frequency. A damping term is introduced into the rod formulation by using a complex Young's modulus. It is defined as $E_c=E(1+\mathrm{i}\eta)$, where η is the hysteretic structural damping loss factor and $\mathrm{i}=\sqrt{-1}$. The general solution to Eq. (3) can be expressed using arbitrary constants $\mathbf{A}$ and $\mathbf{B}$ as

$$\widehat{u}(x)=\mathbf{A}\,\mathrm{e}^{-\mathrm{i}kx}+\mathbf{B}\,\mathrm{e}^{-\mathrm{i}k(L-x)}, \tag{4}$$

where L is the rod element length, k is the complex wavenumber given by

$$k=\frac{\omega}{c}, \tag{5}$$

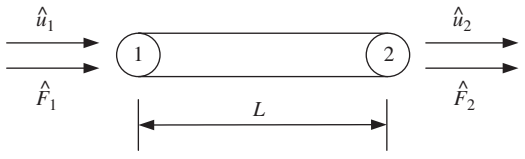

Fig. 1. Nodal displacements and forces for two-node rod elements under axial loading.

and c is the phase speed in the rod,

$$c = \sqrt{\frac{E_c}{\rho}}. \tag{6}$$

The constants **A** and **B** in Eq. (4) are determined by the boundary conditions of the rod. The displacement end conditions for the two-noded element are

$$\widehat{u}(0) \equiv \widehat{u}_1 = \mathbf{A} + \mathbf{B}\,\mathrm{e}^{-\mathrm{i}kL}, \tag{7}$$

$$\widehat{u}(L) \equiv \widehat{u}_2 = \mathbf{A}\,\mathrm{e}^{-\mathrm{i}kL} + \mathbf{B}, \tag{8}$$

where $\widehat{u}_1$ and $\widehat{u}_2$ are the nodal displacements at the rod element node numbers 1 and 2, respectively. By rewriting Eqs. (7) and (8) in a matrix form and solving for **A** and **B** in terms of nodal displacements, one has

$$\begin{Bmatrix} \mathbf{A} \\ \mathbf{B} \end{Bmatrix} = \begin{bmatrix} 1 & \mathrm{e}^{-\mathrm{i}kL} \\ \mathrm{e}^{-\mathrm{i}kL} & 1 \end{bmatrix}^{-1} \begin{Bmatrix} \widehat{u}_1 \\ \widehat{u}_2 \end{Bmatrix}. \tag{9}$$

From Eqs. (2) the loads at the rod element nodes are

$$\widehat{F}_1 = -\widehat{F}(0) = -ES[-\mathrm{i}k\mathbf{A} + \mathrm{i}k\mathbf{B}\,\mathrm{e}^{-\mathrm{i}kL}], \tag{10}$$

$$\widehat{F}_2 = \widehat{F}(L) = ES[-\mathrm{i}k\mathbf{A}\,\mathrm{e}^{-\mathrm{i}kL} + \mathrm{i}k\mathbf{B}], \tag{11}$$

which can be rewritten in matrix form as

$$\begin{Bmatrix} \widehat{F}_1 \\ \widehat{F}_2 \end{Bmatrix} = ES \begin{bmatrix} \mathrm{i}k & -\mathrm{i}k\,\mathrm{e}^{-\mathrm{i}kL} \\ -\mathrm{i}k\mathrm{e}^{-\mathrm{i}kL} & \mathrm{i}k \end{bmatrix} \begin{Bmatrix} \mathbf{A} \\ \mathbf{B} \end{Bmatrix}. \tag{12}$$

Substituting Eq. (9) in Eq. (12), the dynamic stiffness matrix for the two-noded rod element, $\widehat{K}_S$, can be obtained as

$$\begin{Bmatrix} \widehat{F}_1 \\ \widehat{F}_2 \end{Bmatrix} = \underbrace{\frac{ES}{L}\frac{\mathrm{i}kL}{(1-\mathrm{e}^{-\mathrm{i}2kL})} \begin{bmatrix} 1+\mathrm{e}^{-\mathrm{i}2kL} & -2\,\mathrm{e}^{-\mathrm{i}2kL} \\ -2\,\mathrm{e}^{-\mathrm{i}2kL} & 1+\mathrm{e}^{-\mathrm{i}2kL} \end{bmatrix}}_{\widehat{K}_S} \begin{Bmatrix} \widehat{u}_1 \\ \widehat{u}_2 \end{Bmatrix}. \tag{13}$$

For harmonic excitation, the time-averaged energy density for longitudinal waves in a rod can be written as a summation of the potential and kinetic energy densities,

$$\langle e \rangle = \frac{1}{4}ES\left\{\frac{\partial \widehat{u}}{\partial x}\frac{\partial \widehat{u}^*}{\partial x}\right\} + \frac{1}{4}\rho S\left\{\frac{\partial \widehat{u}}{\partial t}\frac{\partial \widehat{u}^*}{\partial t}\right\}, \tag{14}$$

where $\langle\,\rangle$ and $*$ represent the time-averaged quantity and the complex conjugate, respectively. The time-averaged energy flow for longitudinal waves in a rod is given by

$$\langle q \rangle = \frac{1}{2}\mathrm{Re}\left\{-\widehat{F}\frac{\partial \widehat{u}^*}{\partial t}\right\}, \tag{15}$$

where Re is the real part of a complex number.

A complete formulation for beams and other types of spectral elements can be found in Refs. [7,10]. Since the SEM is based upon an exact solution of the wave equation, in this work it will be used as reference to compare it with the distribution of energy density and energy flow calculated by the proposed ESEM method.

3. Energy spectral element method

The ESEM is obtained by applying the same matrix methodology of the spectral element to the governing approximated energy equation for one-dimensional structural elements (i.e., rods and beams). The energy balance in a one-dimensional differential element shows that the time rate of the change of energy inside the element must be equal to the net energy flow through the element minus the power dissipated within the element. The resulting energy balance can be written as [2]

$$\frac{\partial e}{\partial t} = -\frac{\partial q}{\partial x} - \pi_{\text{diss}}, \tag{16}$$

where e is the energy density per unit length, q is the energy flow, and π_{diss} is the power dissipated due to internal damping. For steady-state conditions, the time derivative of energy density is zero.

It is common to consider that the time-averaged power dissipated inside a structure is proportional to the local energy density [1], so

$$\langle \pi_{\text{diss}} \rangle = \eta \omega \langle e \rangle. \tag{17}$$

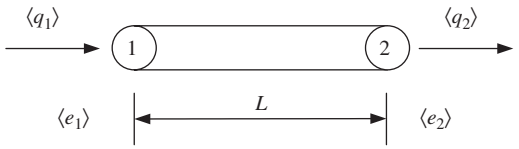

Fig. 2. Nodal energy flows and energy densities for two-node elements borne by longitudinal waves.

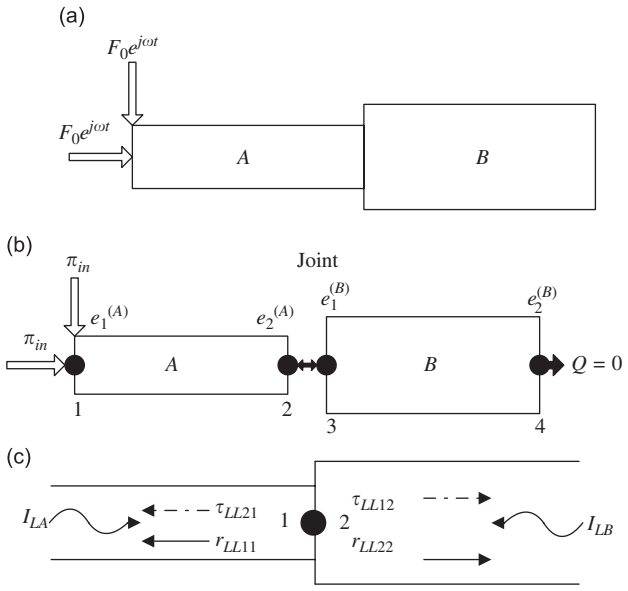

Fig. 3. Two collinear coupling elements: (a) force–displacement model; (b) energy flow equivalent model; (c) semi-infinite rod joint element model.

For a finite structure, energy flow and energy density are related by [3]

$$\langle q\rangle = -\frac{c_g^2}{\eta\omega}\frac{\partial\langle e\rangle}{\partial x}, \tag{18}$$

where $\langle q\rangle$ is the time-averaged energy flow, $\langle e\rangle$ is the time-averaged energy density, and c_g is the group speed of the type of wave propagating in the structure. The expressions of group speed for longitudinal (rod) and flexural (beam) waves are, respectively,

$$c_{\mathrm{gl}} = \sqrt{\frac{E_c S}{\rho S}}, \quad c_{\mathrm{gf}} = 2\left[\frac{\omega^2 E_c I}{\rho S}\right]^{1/4}. \tag{19}$$

By substituting Eqs. (17) and (18) in Eq. (16), the approximate governing energy equations for one-dimensional elements with a small structural damping loss factor ($\eta \ll 1$) is obtained as

$$-\frac{c_g^2}{\eta\omega}\nabla^2\langle e\rangle + \eta\omega\langle e\rangle = 0. \tag{20}$$

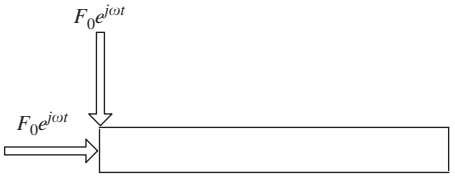

Fig. 4. One-dimensional single structures.

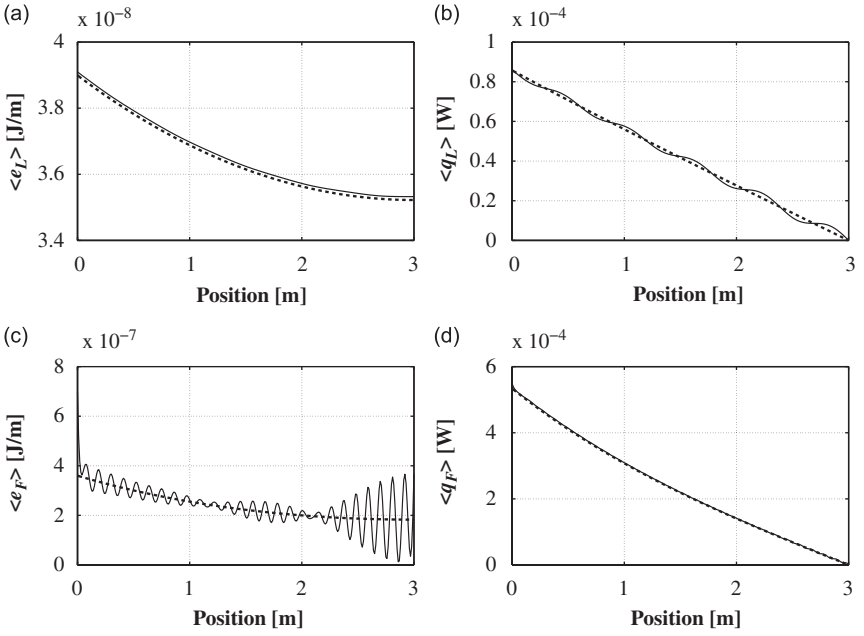

Fig. 5. Longitudinal energy: (a) density and (b) flow, and flexural energy; (c) density and (d) flow, obtained by (- - -) ESEM and (—) SEM for a one-dimensional simple structure with $L = 3.0\,\mathrm{m}$ and $f_c = 4.0\,\mathrm{kHz}$.

The general solution of Eq. (20) can be written as

$$\langle e \rangle = \mathbf{H}\, e^{\eta k x} + \mathbf{G}\, e^{-\eta k x}, \tag{21}$$

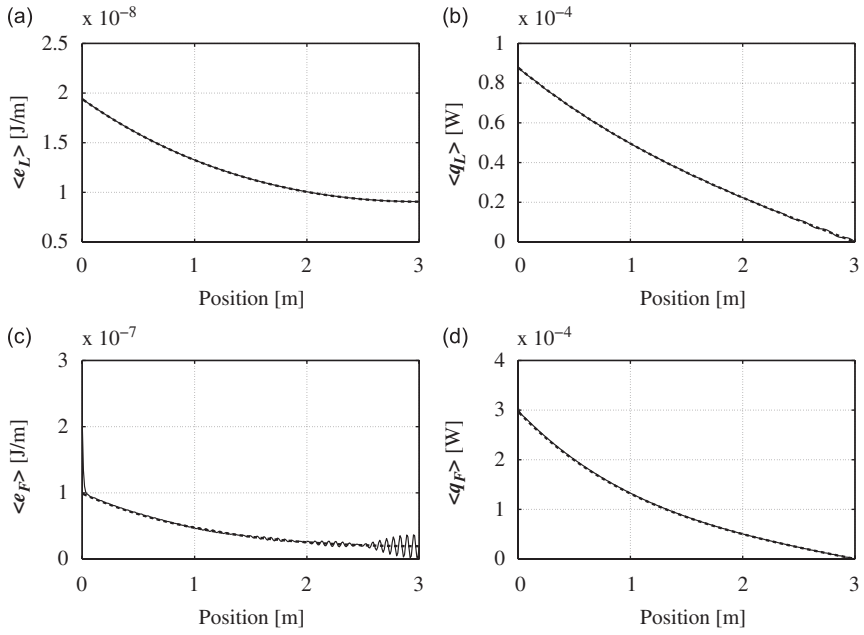

Fig. 6. Longitudinal energy: (a) density and (b) flow, and flexural energy: (c) density and (d) flow, obtained by (– – –) ESEM and (—) SEM for a one-dimensional simple structure with $L = 3.0\,\mathrm{m}$ and $f_c = 12.5\,\mathrm{kHz}$.

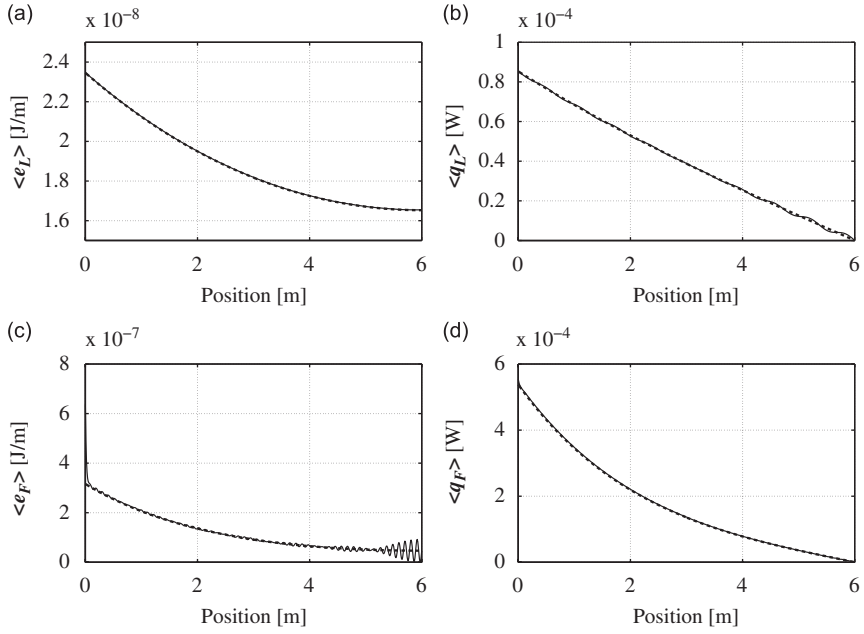

Fig. 7. Longitudinal energy: (a) density and (b) flow, and flexural energy: (c) density and (d) flow, obtained by (– – –) ESEM and (—) SEM for a one-dimensional simple structure with $L = 6.0\,\mathrm{m}$ and $f_c = 4.0\,\mathrm{kHz}$.

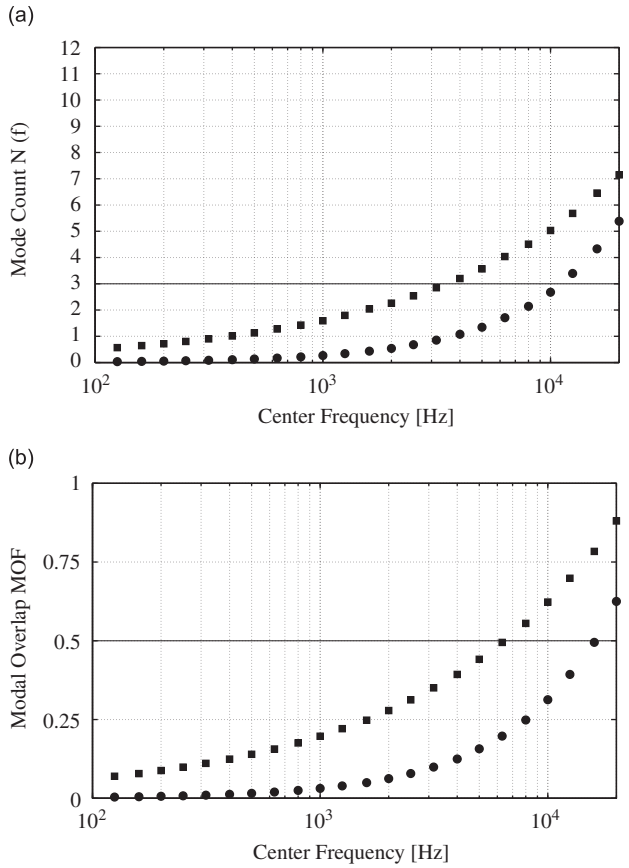

Fig. 8. Validity region of ESEM for element A as (•) rod and (■) beam by: (a) mode count ($N(f)$) and (b) overlap modal factor (MOF) versus center frequency, (−) validity criteria.

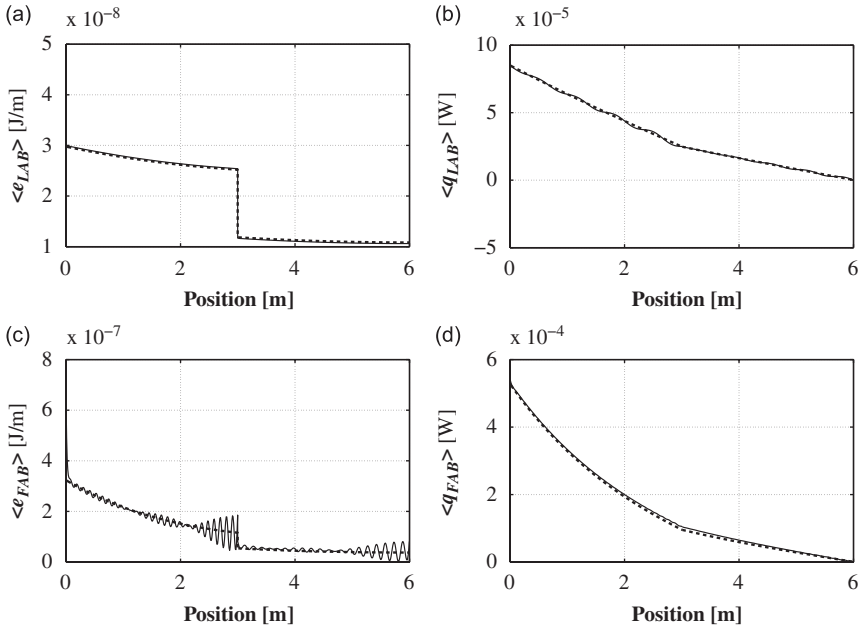

Fig. 9. Longitudinal energy: (a) density and (b) flow, and flexural energy: (c) density and (d) flow, obtained by (- - -) ESEM and (—) SEM for a two collinear coupled structure with $f_c = 4.0\,\text{kHz}$.

where L is the element length, and $\mathbf{H}$ and $\mathbf{G}$ are arbitrary constants determined by the boundary conditions. It must be emphasized that the difference in this solution for longitudinal and flexural waves will be the group speed.

Fig. 2 shows an elastic two-noded one-dimensional energy spectral element with uniform cross-section subjected to energy flow $\langle q_1 \rangle$ and $\langle q_2 \rangle$ at the element nodes 1 and 2, respectively. By applying the energy density boundary conditions at element nodes 1 and 2, the following equations are obtained:

$$\langle e_1 \rangle = \langle e(0) \rangle = \mathbf{H} + \mathbf{G}, \tag{22}$$

$$\langle e_2 \rangle = \langle e(L) \rangle = \mathbf{H}\, e^{\eta k L} + \mathbf{G}\, e^{-\eta k L}, \tag{23}$$

which can be rewritten in matrix form and solved for $\mathbf{H}$ and $\mathbf{G}$ in terms of energy densities as

$$\begin{Bmatrix} \mathbf{H} \\ \mathbf{G} \end{Bmatrix} = \begin{bmatrix} 1 & 1 \\ e^{\eta k L} & e^{-\eta k L} \end{bmatrix}^{-1} \begin{Bmatrix} \langle e_1 \rangle \\ \langle e_2 \rangle \end{Bmatrix}. \tag{24}$$

Applying the energy flow end conditions at element nodes 1 and 2 results in

$$\langle q_1 \rangle = \langle q(0) \rangle = -\frac{c_g^2}{\eta \omega} [\eta k \mathbf{H} - \eta k \mathbf{G}], \tag{25}$$

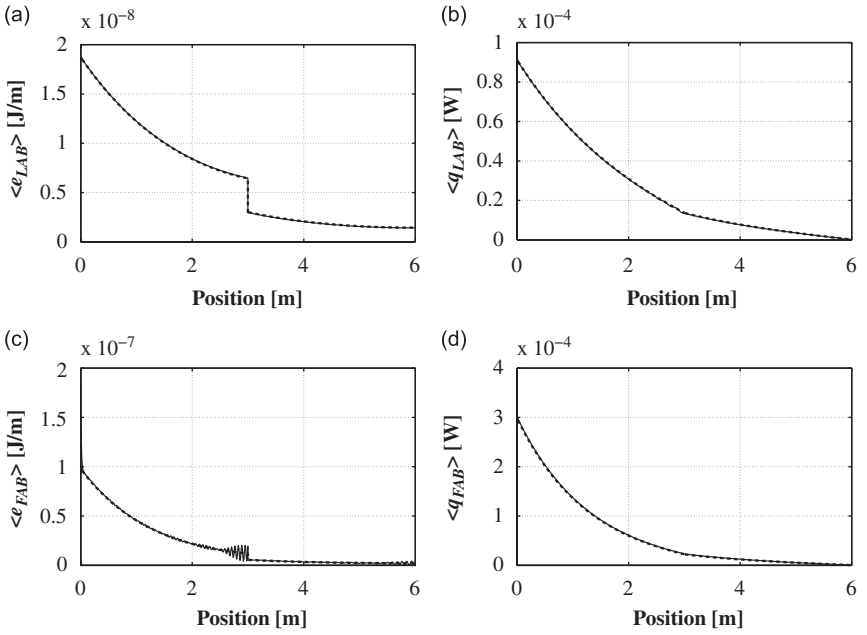

Fig. 10. Longitudinal energy: (a) density and (b) flow, and flexural energy: (c) density and (d) flow, obtained by (– – –) ESEM and (—) SEM for a two collinear coupled structure with $f_c = 12.5\,\text{kHz}$.

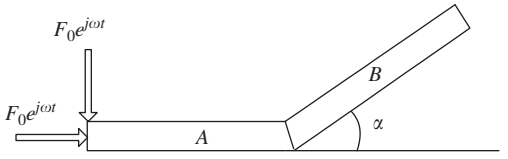

Fig. 11. Two coupled beams at arbitrary angles excited by longitudinal and transversal harmonic point forces.

$$\langle q_2 \rangle = -\langle q(L) \rangle = \frac{c_g^2}{\eta\omega}[\eta k \mathbf{H}\, \mathrm{e}^{\eta k L} - \eta k \mathbf{G}\, \mathrm{e}^{-\eta k L}], \tag{26}$$

which can be rewritten in matrix form as

$$\begin{Bmatrix} \langle q_1 \rangle \\ \langle q_2 \rangle \end{Bmatrix} = \frac{c_g^2}{\eta\omega} \begin{bmatrix} -\eta k & \eta k \\ \eta k\, \mathrm{e}^{\eta k L} & -\eta k\, \mathrm{e}^{-\eta k L} \end{bmatrix} \begin{Bmatrix} \mathbf{H} \\ \mathbf{G} \end{Bmatrix}. \tag{27}$$

By substituting Eq. (24) in Eq. (27) the one-dimensional spectral energy flow matrix, K_E, is obtained as

$$\begin{Bmatrix} \langle q_1 \rangle \\ \langle q_2 \rangle \end{Bmatrix} = \underbrace{\frac{c_g}{(1 - \mathrm{e}^{2\eta k L})} \begin{bmatrix} 1 + \mathrm{e}^{2\eta k L} & -2\, \mathrm{e}^{\eta k L} \\ -2\, \mathrm{e}^{\eta k L} & 1 + \mathrm{e}^{2\eta k L} \end{bmatrix}}_{K_E} \begin{Bmatrix} \langle e_1 \rangle \\ \langle e_2 \rangle \end{Bmatrix}. \tag{28}$$

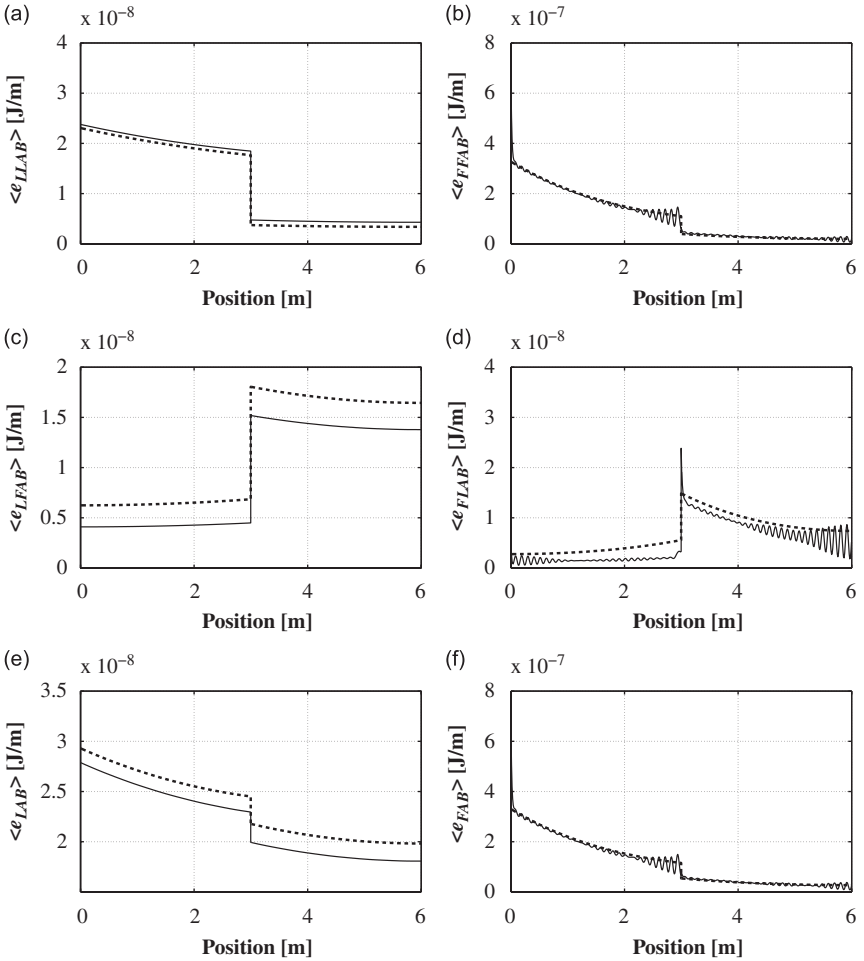

Fig. 12. Energy densities: partial longitudinal from (a) longitudinal and (c) flexural wave; partial flexural from (b) flexural and (d) longitudinal wave; total (e) longitudinal and (f) flexural obtained by (– – –) ESEM and (—) SEM for a two coupled structure with 60° for a 1/3-octave frequency band with $f_c = 4.0$ kHz.

4. Structural coupling model

Generally, built-up structures present discontinuities such as changes in material, geometry or structural configurations which modify the wave propagation behavior (Fig. 3a). To account for these discontinuities, additional energy coupling relationships need to be formulated and inserted at these connection points (Fig. 3b). Joint elements can be obtained for any coupled structural elements, since the energy transmission between them can be described in terms of power transmission and reflection coefficients [11]. The joint elements used in this study were proposed by Cho [3], and are used here for the following structural coupling types: rod–rod collinear, beam–beam collinear, and beam–beam at an arbitrary angle. However, only the formulation for the rod–rod collinear coupling will be presented here; formulations for other one-dimensional coupling joint elements can be obtained following a similar procedure.

The process of transmission and reflection of waves at a joint of a finite structure (Fig. 3b) can be described locally by a semi-infinite rod joint model (Fig. 3c). There are two coincident nodes where, on the left-hand side of the joint, node 1 is part of element A, and, on the right-hand side of the joint, node 2 is part of element B. In this joint model, a left propagating wave (I_B) incident upon the joint is partially reflected and partially transmitted, and a right propagating wave (I_A) incident upon the joint is also partially reflected and transmitted. Therefore, the left propagating energy flow in rod A can be represented by the sum of the contributions from the partially reflected right propagating wave in rod A and the partially transmitted left

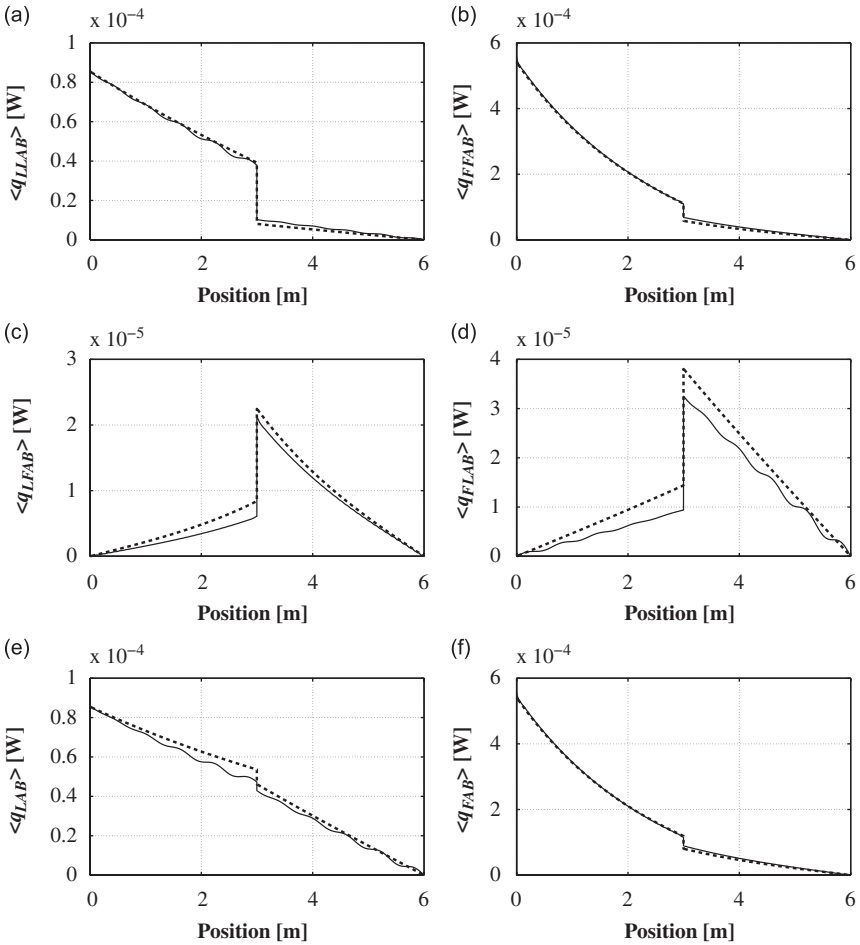

Fig. 13. Energy flows: partial longitudinal from (a) longitudinal and (c) flexural wave; partial flexural from (b) flexural and (d) longitudinal wave; total (e) longitudinal and (f) flexural obtained by (– – –) ESEM and (—) SEM for a two coupled structure with 60° for a 1/3-octave frequency band with $f_c = 4.0$ kHz.

propagating wave in rod B. The right propagating energy flow in rod B can be represented by the sum of contributions from the partially reflected left propagating wave in rod B and the partially transmitted right propagating wave in rod A. Thus, the contributions of energy flow can be determined in terms of the power transmission and reflection coefficients in each rod, and the net energy flow away from the joint at each node can be expressed as

$$\langle q_1\rangle^- = r_{LL11}\langle q_1\rangle^+ + \tau_{LL21}\langle q_2\rangle^+, \tag{29}$$

$$\langle q_2\rangle^- = \tau_{LL12}\langle q_1\rangle^+ + r_{LL22}\langle q_2\rangle^+, \tag{30}$$

where τ_{LLij} is the longitudinal wave power transmission coefficient from node i to node j and r_{LLii} is the longitudinal wave power reflection coefficient at node i. As a signal convention, energy flow incident upon the joint is positive and the reverse is negative, based on the one-dimensional reciprocity relationship $\tau_{LLij} = \tau_{LLji}$ and $r_{LLii} = r_{LLjj}$, which means that only one set of power coefficients needs to be calculated. Since this joint model is conservative $\tau_{LLij} + r_{LLii} = 1$, and the addition of Eqs. (29) and (30) produces the joint energy flow balance relationship,

$$\langle q_1\rangle^+ - \langle q_1\rangle^- = \langle q_2\rangle^+ - \langle q_2\rangle^-. \tag{31}$$

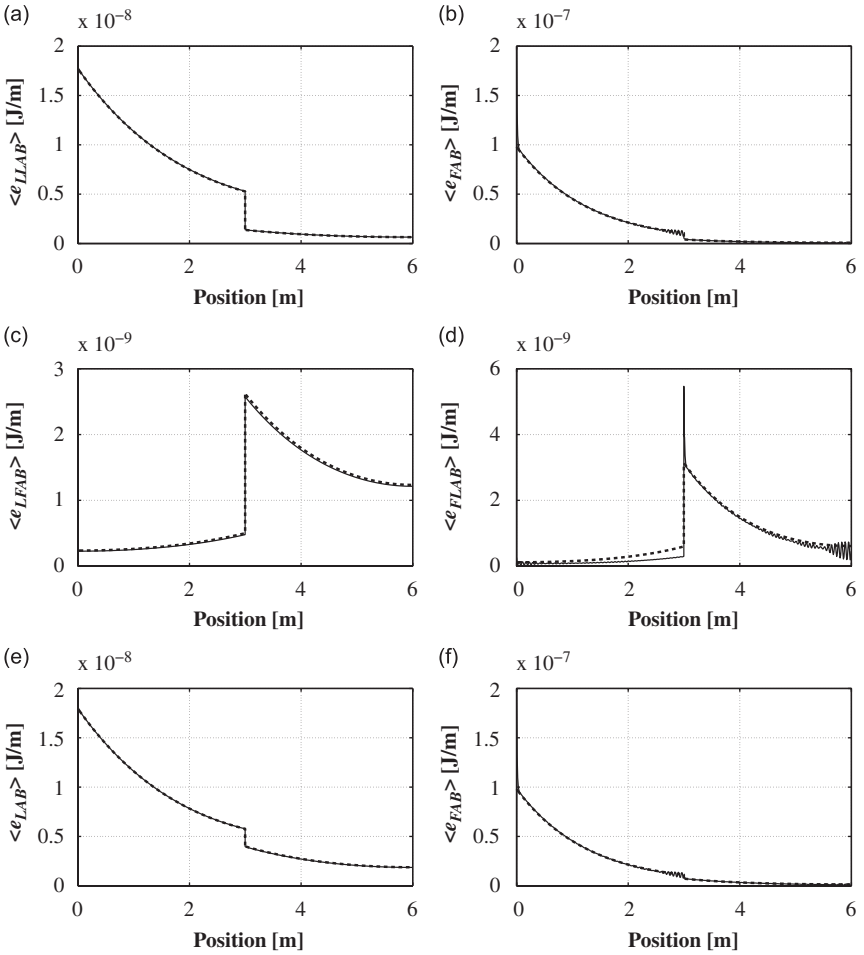

Fig. 14. Energy densities: partial longitudinal from (a) longitudinal and (c) flexural wave; partial flexural from (b) flexural and (d) longitudinal wave; total (e) longitudinal and (f) flexural obtained by (– – –) ESEM and (—) SEM for a two coupled structure with 60° for a 1/3-octave frequency band with $f_c = 12.5$ kHz.

The resulting energy flow at the joint is the difference between the negative (moving out of the joint) and positive (moving into the joint) energy flows, which can be written in terms of the joint nodes 1 and 2, respectively, as

$$\langle q_1 \rangle = \langle q_1 \rangle^+ - \langle q_1 \rangle^-, \tag{32}$$

$$\langle q_2 \rangle = \langle q_2 \rangle^+ - \langle q_2 \rangle^-. \tag{33}$$

From Eqs. (18) and (21) it is possible to show that Eqs. (32) and (33) become,

$$\langle q_1 \rangle = c_{\mathrm{gla}} \langle e_1 \rangle^+ - c_{\mathrm{gla}} \langle e_1 \rangle^-, \tag{34}$$

$$\langle q_2 \rangle = c_{\mathrm{glb}} \langle e_2 \rangle^+ - c_{\mathrm{glb}} \langle e_2 \rangle^-. \tag{35}$$

Substituting Eqs. (29) and (34) in Eq. (32), and Eqs. (30) and (35) in Eq. (33), the following relationships are obtained:

$$\langle q_1 \rangle = c_{\mathrm{gla}}(1 - r_{LL11}) \langle e_1 \rangle^+ - c_{\mathrm{glb}} \tau_{LL21} \langle e_2 \rangle^+, \tag{36}$$

$$\langle q_2 \rangle = -c_{\mathrm{gla}} \tau_{LL21} \langle e_1 \rangle^+ + c_{\mathrm{glb}}(1 - r_{LL22}) \langle e_2 \rangle^+. \tag{37}$$

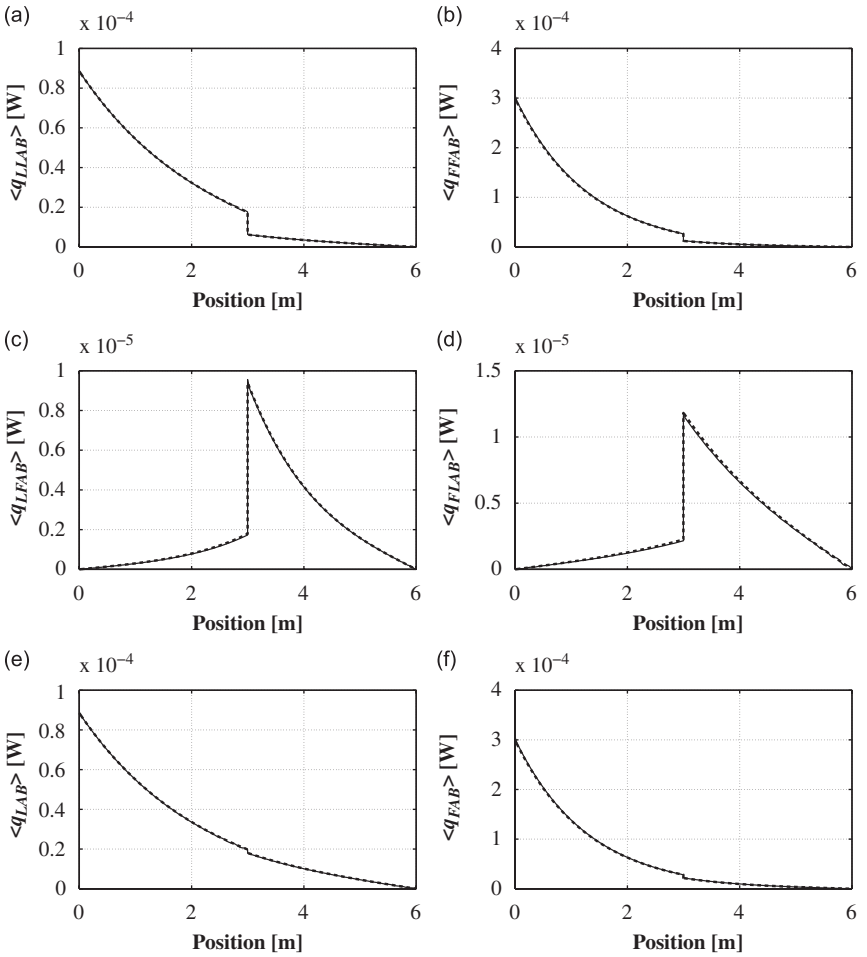

Fig. 15. Energy flows: partial longitudinal from (a) longitudinal and (c) flexural wave; partial flexural from (b) flexural and (d) longitudinal wave; total (e) longitudinal and (f) flexural obtained by (- - -) ESEM and (—) SEM for a two coupled structure with 60° for a 1/3-octave frequency band with $f_c = 12.5$ kHz.

Eqs. (36) and (37) can be rewritten in matrix form as

$$\begin{Bmatrix} \langle q_1 \rangle \\ \langle q_2 \rangle \end{Bmatrix} = \underbrace{\begin{bmatrix} c_{\mathrm{gla}}(1 - r_{LL11}) & -c_{\mathrm{glb}}\tau_{LL21} \\ -c_{\mathrm{gla}}\tau_{LL21} & c_{\mathrm{glb}}(1 - r_{LL22}) \end{bmatrix}}_{P} \begin{Bmatrix} \langle e_1 \rangle^+ \\ \langle e_2 \rangle^+ \end{Bmatrix}. \tag{38}$$

The values of energy density at the joint nodes can also be expressed in terms of energy density components moving in the positive and negative directions. Hence, the total energy densities at the coupling nodes are given by

$$\langle e_1 \rangle = \langle e_1 \rangle^+ + \langle e_1 \rangle^-, \tag{39}$$

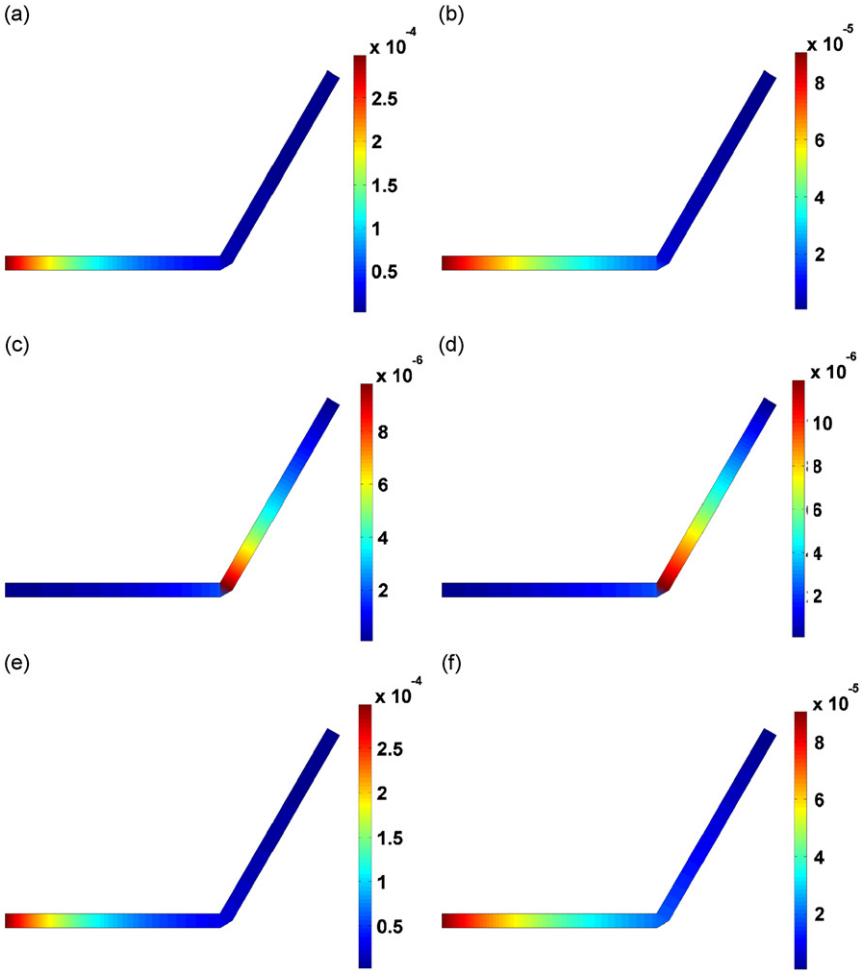

Fig. 16. New graphic representation of Fig. 15.

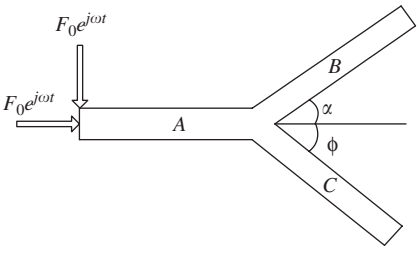

Fig. 17. Branched beams.

$$\langle e_2\rangle = \langle e_2\rangle^+ + \langle e_2\rangle^-. \tag{40}$$

The nodal values of energy density, Eqs. (39) and (40), must also be expressed in terms of the relationship given by Eqs. (29), (30), and (35). Thus, the new relationships for total energy densities are

$$\langle e_1\rangle = (1 + r_{LL11})\langle e_1\rangle^+ + \frac{c_{\mathrm{glb}}}{c_{\mathrm{gla}}}\tau_{LL21}\langle e_2\rangle^+, \tag{41}$$

$$\langle e_2\rangle = \frac{c_{\mathrm{gla}}}{c_{\mathrm{glb}}}\tau_{LL12}\langle e_1\rangle^+ + (1 + r_{LL22})\langle e_2\rangle^+. \tag{42}$$

Eqs. (41) and (42) can be rewritten in matrix form and solved for $\langle e_1\rangle^+$ and $\langle e_2\rangle^+$ in terms of $\langle e_1\rangle$ and $\langle e_2\rangle$ as

$$\begin{Bmatrix} \langle e_1\rangle^+ \\ \langle e_2\rangle^+ \end{Bmatrix} = \underbrace{\begin{bmatrix} 1 + r_{LL11} & \dfrac{c_{\mathrm{glb}}}{c_{\mathrm{gla}}}\tau_{LL21} \\ \dfrac{c_{\mathrm{gla}}}{c_{\mathrm{glb}}}\tau_{LL12} & 1 + r_{LL22} \end{bmatrix}^{-1}}_{E^{-1}} \begin{Bmatrix} \langle e_1\rangle \\ \langle e_2\rangle \end{Bmatrix}. \tag{43}$$

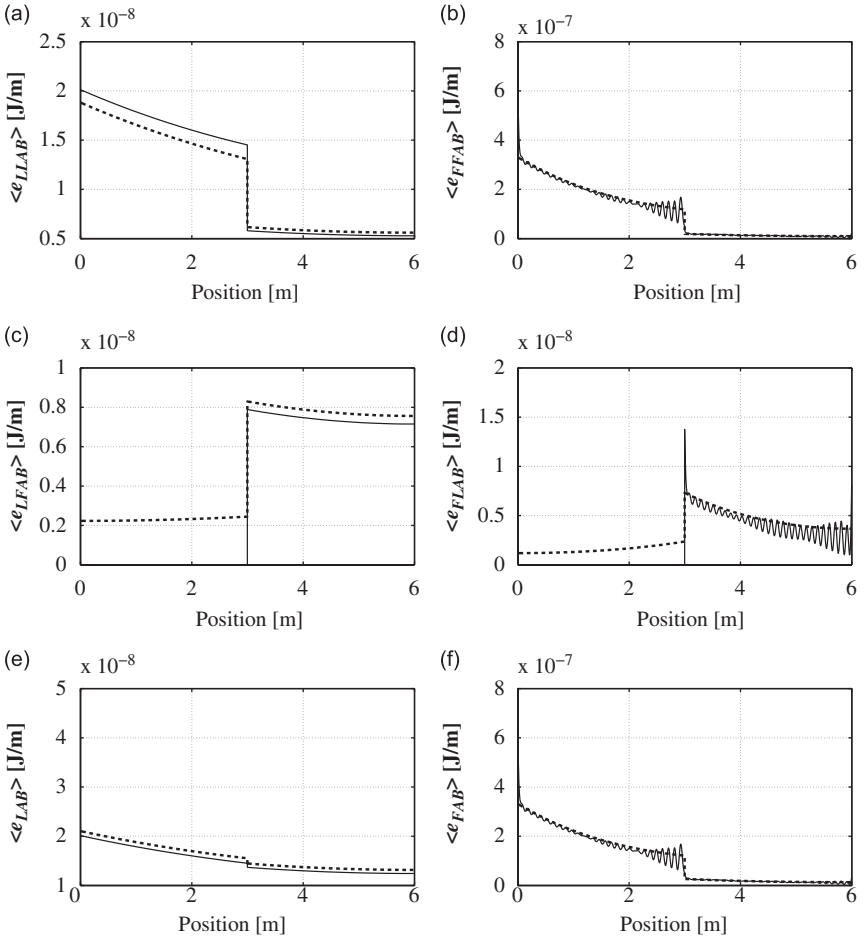

Fig. 18. Energy densities: partial longitudinal from (a) longitudinal and (c) flexural wave; partial flexural from (b) flexural and (d) longitudinal wave; total (e) longitudinal and (f) flexural obtained by (– – –) ESEM and (—) SEM for the AB branch of three coupled structure with -60° for a 1/3-octave frequency band with $f_c = 4.0\,\mathrm{kHz}$.

By substituting Eq. (43) in Eq. (38) and applying the reciprocity relationship, the rod–rod collinear coupling relationship between the nodal values of energy flow in terms of energy density is obtained as

$$\left\{ \begin{array}{c} \langle q_1 \rangle \\ \langle q_2 \rangle \end{array} \right\} = \underbrace{\frac{\tau_{LL12}}{2r_{LL11}} \left[\begin{array}{cc} c_{\mathrm{gla}} & -c_{\mathrm{glb}} \\ -c_{\mathrm{gla}} & c_{\mathrm{glb}} \end{array} \right]}_{J} \left\{ \begin{array}{c} \langle e_1 \rangle \\ \langle e_2 \rangle \end{array} \right\}. \tag{44}$$

A similar equation can be obtained for the beam–beam collinear coupling relationship by replacing in Eq. (44) the longitudinal power transmission and reflection coefficients for the flexural coefficients (τ_{FFij} and r_{FFii}), and the rod group speeds for the beam group speeds (c_{gfa} and c_{gfb}).

In order to obtain the global energy density system of equations for the rod–rod collinear coupling (Fig. 3b), the joint element must be included at the connection and, from Eqs. (28) and (44), it can be written as

$$\left[\begin{array}{cccc} k_{11}^{(A)} & k_{12}^{(A)} & 0 & 0 \\ k_{21}^{(A)} & \left(k_{22}^{(A)} - c_{\mathrm{gla}} \dfrac{\tau_{LL23}}{2r_{LL22}}\right) & \left(c_{\mathrm{glb}} \dfrac{\tau_{LL23}}{2r_{LL22}}\right) & 0 \\ 0 & \left(c_{\mathrm{gla}} \dfrac{\tau_{LL23}}{2r_{LL22}}\right) & \left(k_{11}^{(B)} - c_{\mathrm{glb}} \dfrac{\tau_{LL23}}{2r_{LL22}}\right) & k_{12}^{(B)} \\ 0 & 0 & k_{21}^{(B)} & k_{22}^{(B)} \end{array} \right] \left\{ \begin{array}{c} \langle e_1 \rangle \\ \langle e_2 \rangle \\ \langle e_3 \rangle \\ \langle e_4 \rangle \end{array} \right\} = \left\{ \begin{array}{c} \pi_{\mathrm{in}} \\ 0 \\ 0 \\ 0 \end{array} \right\}, \tag{45}$$

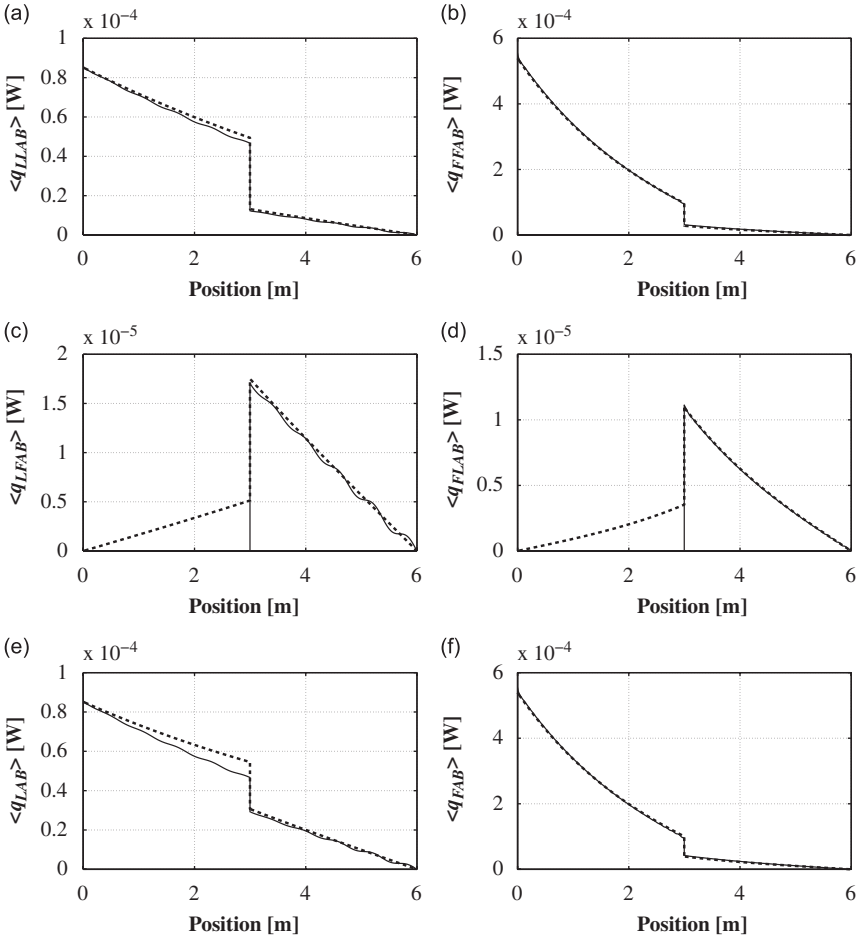

Fig. 19. Energy flows: partial longitudinal from (a) longitudinal and (c) flexural wave; partial flexural from (b) flexural and (d) longitudinal wave; total (e) longitudinal and (f) flexural obtained by (– – –) ESEM and (—) SEM for the AB branch of three coupled structure with -60° for a 1/3-octave frequency band with $f_c = 4.0\,\mathrm{kHz}$.

where π_{in} is the power input on the left end of element A, $\langle e_n \rangle$ are the energy densities at the nodes n, and $k_{ij}^{(m)}$ are the matrix elements of K_E in Eq. (28), with the subscripts i and j indicating the energy spectral element node numbers ($i,\ j = 1,\ 2$) and the superscript (m) indicating the element number.

5. Energetics in one-dimensional structural elements

In order to assess the accuracy of the proposed method, some examples with rod and beam structures are analyzed.

5.1. Single elements

The one-dimensional structural model consists of a traction and flexural element A, with free–free displacement boundary conditions and excited at the left end by a longitudinal and a flexural harmonic force, one at a time, with a magnitude of $F = 1.0\,\mathrm{N}$ (Fig. 4). The structure is made of aluminum ($E = 71.0\,\mathrm{GPa}$ and $\rho = 2700\,\mathrm{kg/m^3}$) with a cross section-area $S = 4 \times 10^{-4}\,\mathrm{m^2}$ and inertia moment $I_{zz} = 1.333 \times 10^{-8}\,\mathrm{m^4}$. The structure's length is $L = 3.0\,\mathrm{m}$ and the structural damping loss factor is $\eta = 0.03$.

The frequency-averaged longitudinal and flexural energy density and energy flow were calculated by ESEM and SEM in a 1/3-octave frequency band with center frequency $f_c = 4.0\,\mathrm{kHz}$. With the exception of the

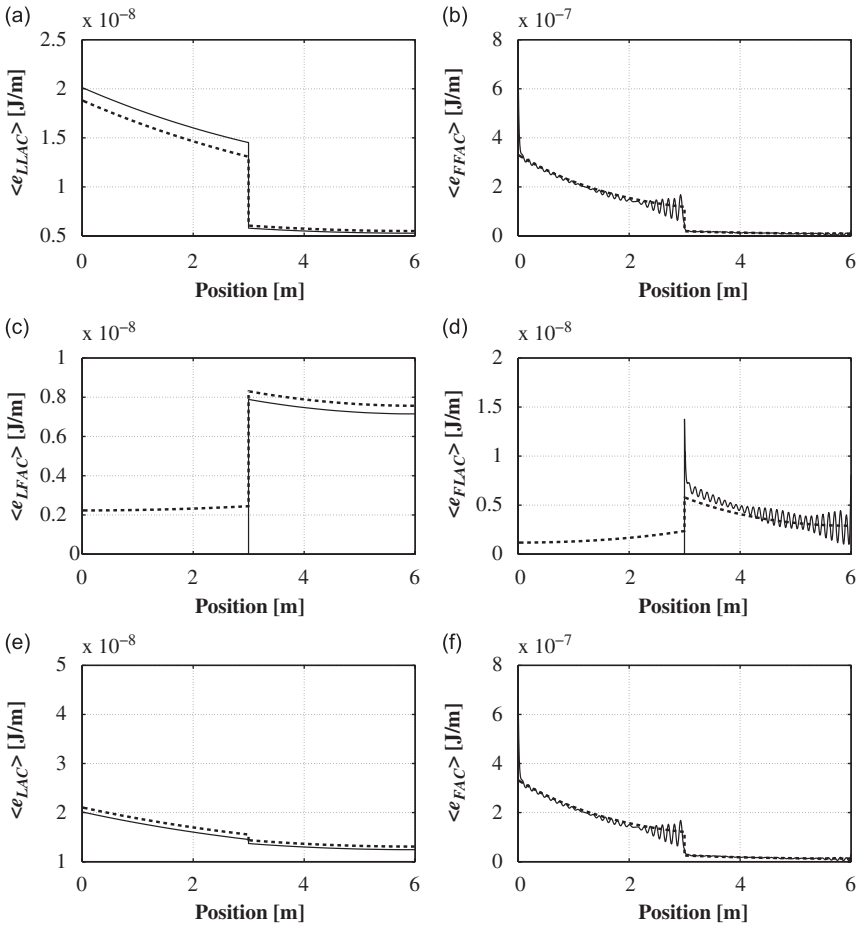

Fig. 20. Energy densities: partial longitudinal from (a) longitudinal and (c) flexural wave; partial flexural from (b) flexural and (d) longitudinal wave; total (e) longitudinal and (f) flexural obtained by (– – –) ESEM and (—) SEM for the AC branch of three coupled structure with 60° for a 1/3-octave frequency band with $f_c = 4.0\,\mathrm{kHz}$.

flexural energy flow (Fig. 5d) none of the other energies calculated by ESEM and SEM (Figs. 5a–c) match exactly. A close examination of the longitudinal energy flow and flexural energy density plots (Figs. 5b and c) reveals that SEM presents a characteristic oscillatory behavior, while ESEM presents a smooth behavior converging to the average values of SEM. This behavior, which was already expected and does not mean a mismatch, comes from the spatial integration included in the ESEM formulation. However, there is still the mismatch of longitudinal energy density (Fig. 5a). For frequency bands with a higher center frequency, e.g., 1/3-octave frequency band with $f_c = 12.5\,\text{kHz}$ (Fig. 6), the results from ESEM and SEM for all energies match. On the other hand, similar results are obtained for the 1/3-octave frequency band with $f_c = 4.0\,\text{kHz}$ if the structure's length is increased to $L = 6.0\,\text{m}$ (Fig. 7).

To obtain quite simple energy flow equations, assumptions and approximations had to be made, which limit the validity region of the method [12]. Derived from experimental deduction, numerical evaluations, and experience, some parameters have been proposed to indicate limits of validity of the methods based on energy formulations. Some of these parameters come from SEA, which uses modal indicators such as mode count, $N(f)$, and the modal overlap factor, MOF [1,9]. Other parameters come from approximate solutions for EFA, such as the energy finite element method (EFEM), which uses wavelength indicators like the nondimensional wavelength parameter (l), the nondimensional wavenumber band (ΔkL) and the nondimensional damped wavenumber band ($\eta\Delta kL$) [3]. Moens [12] showed that modal indicators are related with wavelength indicators and both can be used to validate SEA and EFEM. Since the ESEM provides an exact solution of the energy

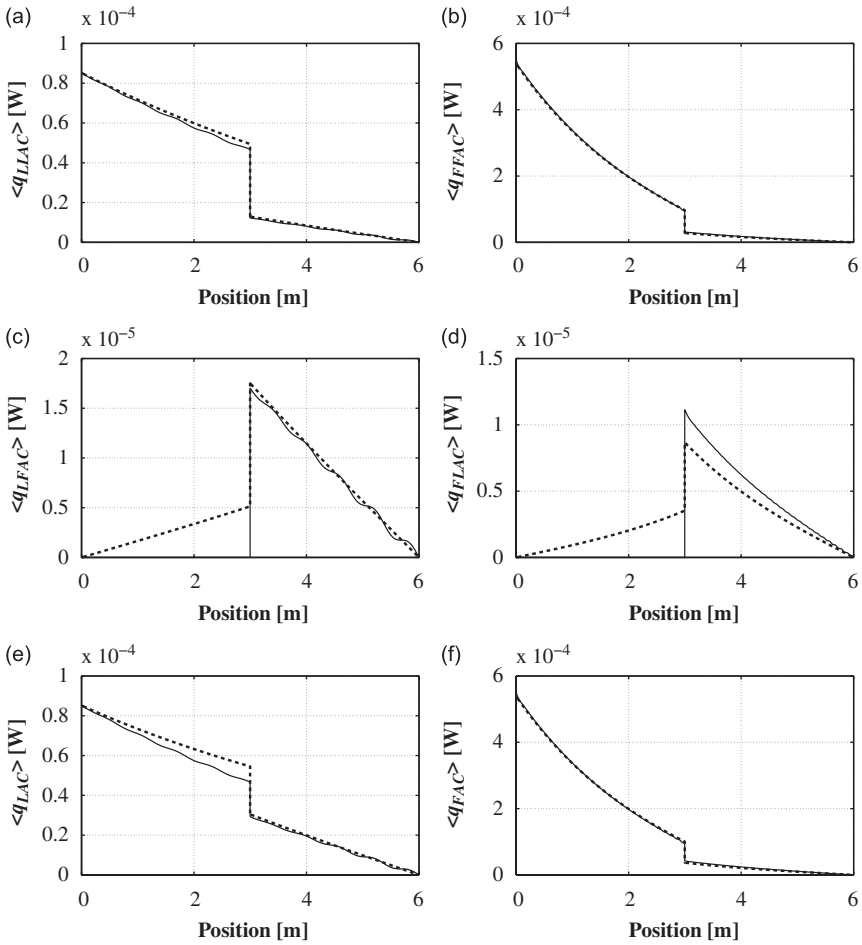

Fig. 21. Energy flows: partial longitudinal from (a) longitudinal and (c) flexural wave; partial flexural from (b) flexural and (d) longitudinal wave; total (e) longitudinal and (f) flexural obtained by (– – –) ESEM and (—) SEM for the AC branch of three coupled structure with 60° for a 1/3-octave frequency band with $f_c = 4.0\,\text{kHz}$.

flow equation and EFEM an approximate one, it will be conservative to use EFEM validity indicators to validate the ESEM. To verify the validity region of ESEM, the mode count and the modal overlap factor were used. The mode count indicates the approximate number of modes excited in the frequency band of interest, and for longitudinal waves it can be written as

$$N(f) = 2\Delta l = 2(l_{\max} - l_{\min}) = 2L\left(\frac{1}{\lambda_{\max}} - \frac{1}{\lambda_{\min}}\right), \tag{46}$$

where Δl is the nondimensional wavelength parameter variation, L is the characteristic dimension of the structure (rod length), and λ_i is the wavelength at the frequency band limits ($i = \max, \min$). The modal overlap factor indicates the spacing between modes in the frequency band of interest and, for longitudinal waves, it can be expressed by

$$MOF = 2\eta l = 2\eta\frac{L}{\lambda}, \tag{47}$$

where λ is the largest wavelength in the frequency band of interest. As suggested by Refs. [1,9] the criterion adopted for the longitudinal and flexural waves was $N(f) > 3.0$ and $MOF > 0.5$.

Fig. 8 shows the validity region of ESEM for element A as a rod and a beam, calculated by $N(f)$ and MOF indicators versus center frequency of 1/3-octave frequency bands, f_c. These results can explain some

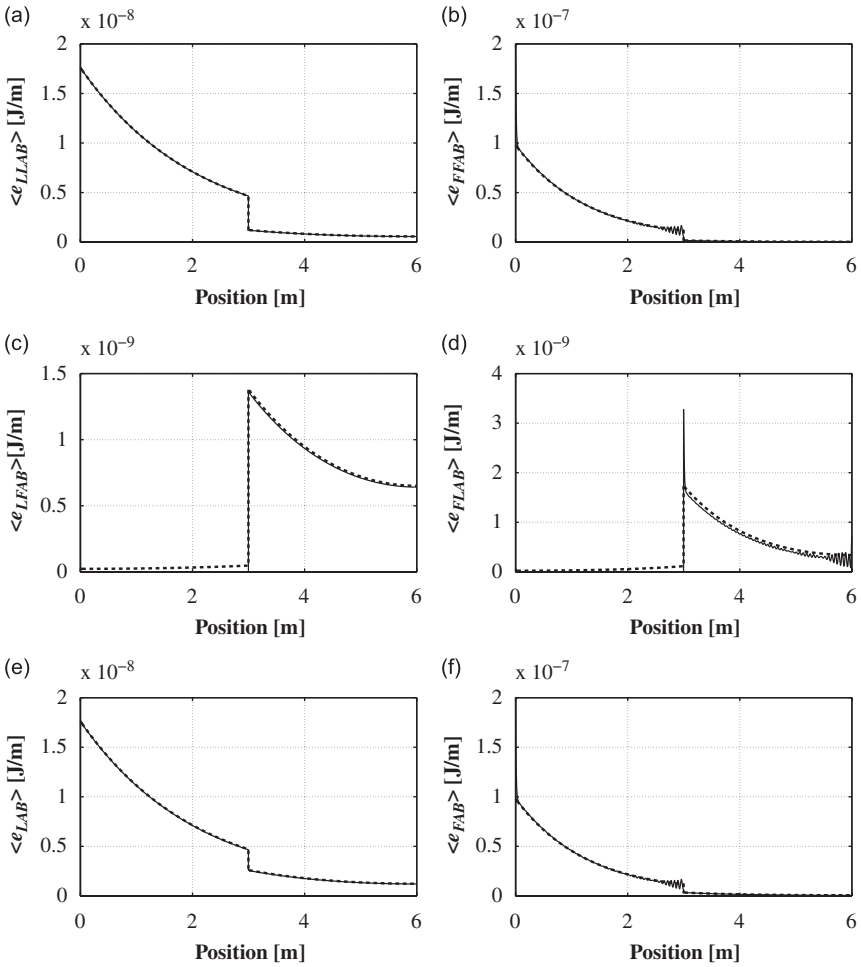

Fig. 22. Energy densities: partial longitudinal from (a) longitudinal and (c) flexural wave; partial flexural from (b) flexural and (d) longitudinal wave; total (e) longitudinal and (f) flexural obtained by (– – –) ESEM and (—) SEM for the AB branch of three coupled structure with -60° for a 1/3-octave frequency band with $f_c = 12.5$ kHz.

mismatches between the energy results from ESEM and SEM. Differences of longitudinal energy density by ESEM and SEM for the 1/3-octave frequency band with $f_c = 4.0\,\text{kHz}$ stem from the fact that the validity indicators ($N(f)$ and MOF) for element A as a rod are below the acceptable limit in this frequency band (Fig. 8). In the frequency band with $f_c = 12.5\,\text{kHz}$, element A as a rod presents valid indicators ($N(f)$ and MOF) and a good agreement between ESEM and SEM was found. These results confirm that ESEM performs as well as SEM, with the upgrade of ESEM yielding smooth results for longitudinal energy flow and flexural energy densities.

5.2. Collinear coupled elements

Here the structure has free–free boundary conditions (Fig. 3a), and is excited with a harmonic point force at the left end in the longitudinal and transversal directions, one at a time, with a magnitude of $F = 1.0\,\text{N}$. Elements A and B are made of aluminum ($E = 71.0\,\text{GPa}$ and $\rho = 2700\,\text{kg/m}^3$) with cross-section areas of $S_A = 4 \times 10^{-4}\,\text{m}^2$ and $S_B = 16 \times 10^{-4}\,\text{m}^2$, lengths $L_A = L_B = 3.0\,\text{m}$, and a structural damping loss factor of $\eta = 0.03$. Frequency-averaged longitudinal and flexural energy densities and energy flows were calculated using ESEM and SEM over a 1/3-octave frequency band with $f_c = 4.0\,\text{kHz}$. Fig. 9 indicates that the results from ESEM and SEM present a similar behavior as the single element case, but with marked difference for

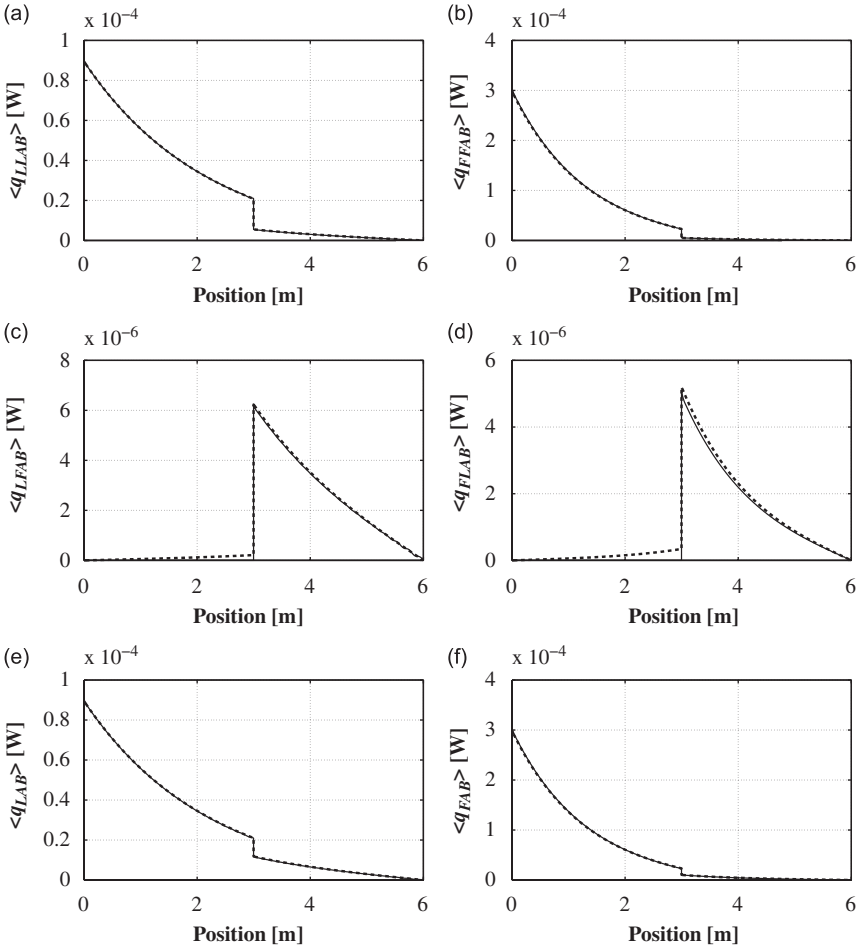

Fig. 23. Energy flows: partial longitudinal from (a) longitudinal and (c) flexural wave; partial flexural from (b) flexural and (d) longitudinal wave; total (e) longitudinal and (f) flexural obtained by (– – –) ESEM and (—) SEM for the AB branch of three coupled structure with -60° for a 1/3-octave frequency band with $f_c = 12.5\,\text{kHz}$.

longitudinal energy density. By moving to a higher frequency band inside the validity region for this problem, the results from ESEM and SEM for the longitudinal and flexural energies present better results, with all energies showing perfect congruence (Fig. 10).

5.3. Coupled elements at arbitrary angle

Fig. 11 shows the configuration for two one-dimensional waveguides connected at an arbitrary angle and excited at the left end by longitudinal and flexural harmonic forces, one at a time, with a magnitude of $F = 1.0\,\mathrm{N}$. The elements are the same A and B as those mentioned in Section 5.2, except that they have equal cross-section areas $S_A = S_B = 4 \times 10^{-4}\,\mathrm{m}^2$. The frequency-averaged longitudinal and flexural energy densities and energy flows were calculated using ESEM and SEM for different angles ranging from 0° to 90°, and for 1/3-octave frequency bands with $f_c = 4.0$ and 12.5 kHz, respectively.

For this coupling type, an exchange of energy will occur between the longitudinal and flexural waves at the joint, and the joint matrix becomes more complicated [3]. To clarify the energy exchange, the total energy of each wave type is calculated in terms of partial energies and analyzed separately. The total longitudinal energy density from waveguide A to waveguide B can be written as $\langle e_{LAB}\rangle = \langle e_{LLAB}\rangle + \langle e_{LFAB}\rangle$, where $\langle e_{LLAB}\rangle$ is the partial longitudinal energy density due to longitudinal wave traveling from waveguide A to B, and $\langle e_{LFAB}\rangle$ is

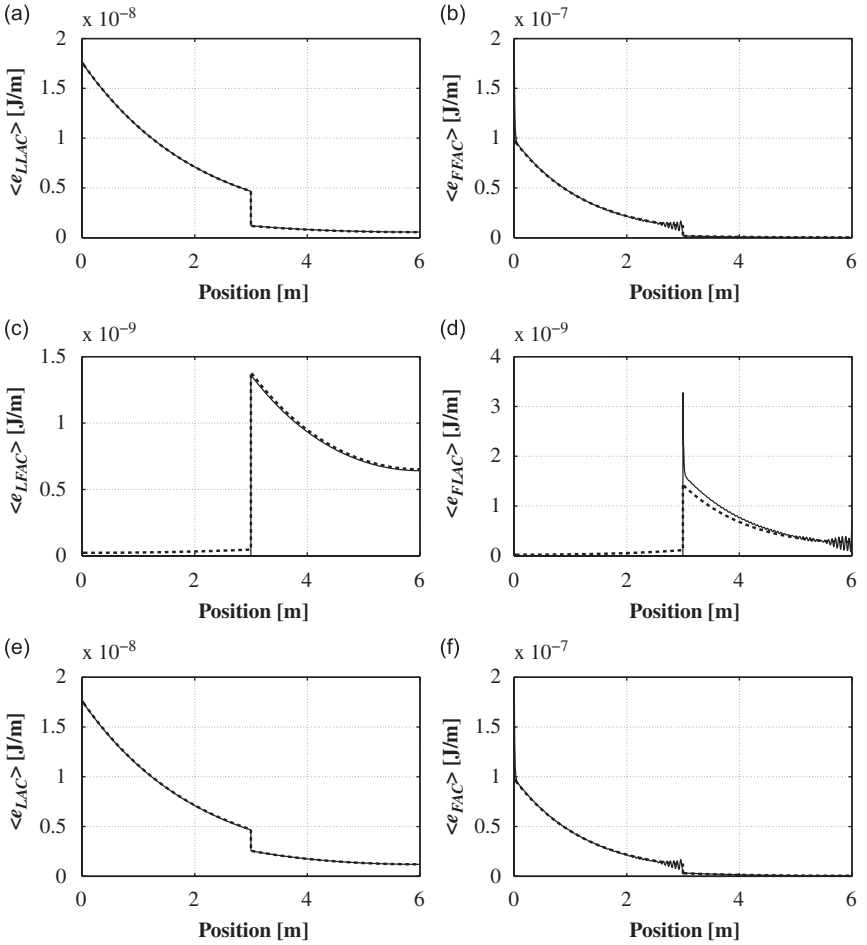

Fig. 24. Energy densities: partial longitudinal from (a) longitudinal and (c) flexural wave; partial flexural from (b) flexural and (d) longitudinal wave; total (e) longitudinal and (f) flexural obtained by (– – –) ESEM and (—) SEM for the AC branch of three coupled structure with 60° for a 1/3-octave frequency band with $f_c = 12.5\,\mathrm{kHz}$.

the partial longitudinal energy density due to flexural wave traveling from waveguide A to B. The same is done for the total flexural energy density as $\langle e_{FAB}\rangle = \langle e_{FFAB}\rangle + \langle e_{FLAB}\rangle$, where $\langle e_{FLAB}\rangle$ is the partial flexural energy density due to longitudinal wave traveling from waveguide A to B, and $\langle e_{FFAB}\rangle$ is the partial flexural energy density due to flexural wave traveling from waveguide A to B. The same concept is used for the energy flow results. Although the problem has been solved for angles ranging from 0° and 90°, only a typical result for 60° is presented here. The results of energy density and flow obtained by ESEM and SEM for 1/3-octave frequency bands with $f_c = 4.0$ kHz are shown in Figs. 12 and 13. As expected, partial and total energy densities and flows do not match exactly. By shifting to a higher frequency band ($f_c = 12.5$ kHz), inside the validity region for ESEM, the results present better agreement for the total energy densities and flows (Figs. 14 and 15), but still show mismatches for some partial energy densities ($\langle e_{LFAB}\rangle$,$\langle e_{FLAB}\rangle$) and flows ($\langle q_{LFAB}\rangle$,$\langle q_{FLAB}\rangle$). These partial energies come from the joint energy exchange between different wave types (longitudinal and flexural). Since the joint model is formulated as a semi-infinite structural element which has been applied to a finite structure, these mismatches may come from these approximations. However, in all the cases analyzed here, the contribution of these partial energies to the total energy is around one to three orders of magnitude lower than that of the other partial energies, which represents a negligible contribution to the total energy. Fig. 16, which shows the same results as Fig. 15, gives a more intuitive graphic representation.

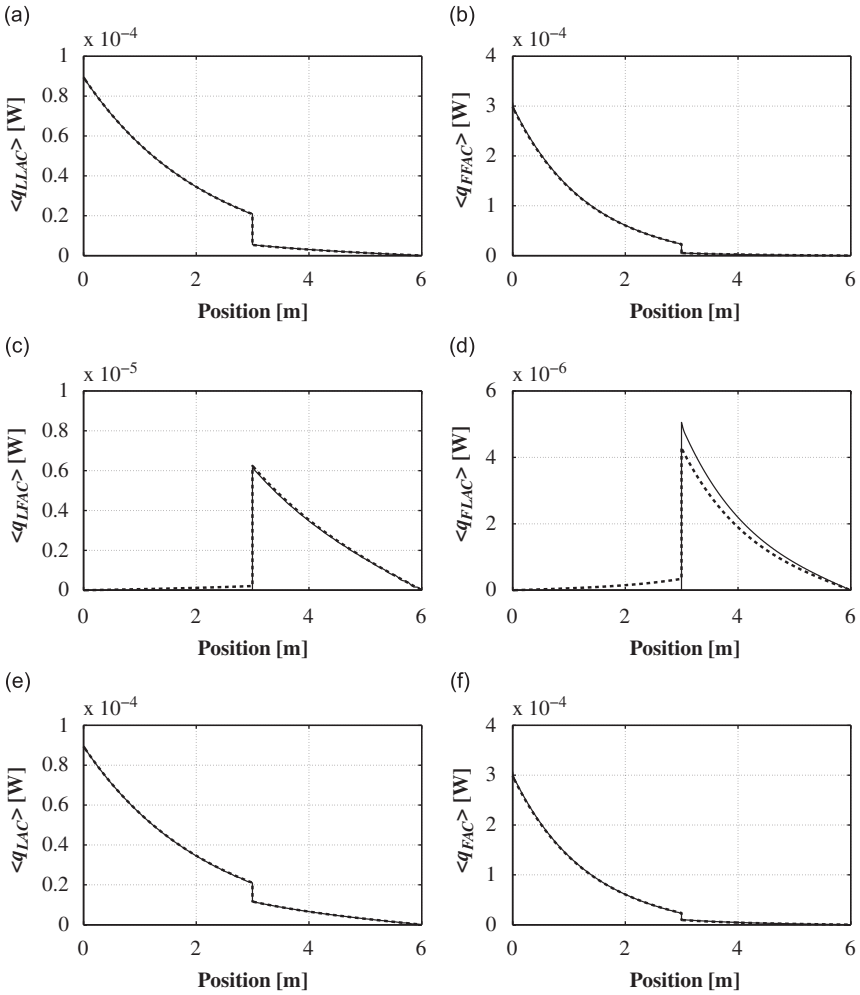

Fig. 25. Energy flows: partial longitudinal from (a) longitudinal and (c) flexural wave; partial flexural from (b) flexural and (d) longitudinal wave; total (e) longitudinal and (f) flexural obtained by (– – –) ESEM and (—) SEM for the AC branch of three coupled structure with 60° for a 1/3-octave frequency band with $f_c = 12.5$ kHz.

5.4. Branched elements

Fig. 17 shows the configuration for three one-dimensional waveguides connected at arbitrary angles and excited at the left end by longitudinal and flexural harmonic forces, one at a time, with a magnitude of $F = 1.0\,\mathrm{N}$. Elements A, B, and C are of the same dimensions, material, and properties as those used for the elements in Section 5.3. The frequency-averaged longitudinal and flexural energy densities and energy flow were calculated using ESEM and SEM for $\alpha = \phi = 60^\circ$, and for 1/3-octave frequency bands with $f_c = 4.0$ and 12.5 kHz, respectively.

The results of energy density and flow obtained by ESEM and SEM for a 1/3-octave frequency band with $f_c = 4.0\,\mathrm{kHz}$ at the AB branch are shown in Figs. 18 and 19, respectively. Similar results for the AC branch are depicted in Figs. 20 and 21. Except for partial and total flexural energy density (Figs. 18b and f) and partial and total flexural energy flow (Figs. 19b and f), none of the other energies calculated by ESEM and SEM exactly match at the AB branch. Similar results were obtained for the AC branch. This behavior was already expected because the validity indicators ($N(f)$ and MOF) for this structure and frequency band are below the limits required for ESEM. By rising to a frequency band in which $f_c = 12.5\,\mathrm{kHz}$, ESEM produces much better results, which can be confirmed by total energy densities and energy flow results at AB branch (Figs. 22 and 23), and at AC branch (Figs. 24 and 25), respectively. It should be noted that there are still mismatches at some partial energies, but because their contribution to the total energy is several orders of magnitude lower than the others, they do not affect the total energy results.

6. Conclusions

A new method called energy spectral element method (ESEM) is proposed. Predictions made with ESEM for one-dimensional structures were verified using an exact solution of the wave equation obtained by the spectral element method (SEM). Different examples were simulated and results obtained by ESEM and SEM were compared. The configurations treated consist of free–free structures composed of single elements, two collinear coupled elements, and two and three coupled elements at arbitrary angles. The main divergences between the energy density and energy flow results obtained with SEM and ESEM stem from the validity limits of ESEM formulation and coupling relationships in the frequency band of interest. ESEM was shown to be suitable for high frequencies, and it produces good results when the analyses are performed inside the validity region for the method, which can be characterized by high mode count ($N(f)$) and high modal overlap factor (MOF) indicators. This work reaffirms the importance of $N(f)$ and MOF as indicators that should be used to establish the limits of validity for energy methods in general and for ESEM in particular. A more intuitive graphic presentation of the energy density and power flow was introduced.

Acknowledgments

The authors gratefully acknowledge the Brazilian research funding agencies: Fundação de Apoio a Pesquisa do Estado de São Paulo—FAPESP, Conselho Nacional de Desenvolvimento Científico e Tecnológico—CNPq, and Coordenação de Aperfeiçoamento de Pessoal de Nível Superior—CAPES for the financial support.

References

[1] R.H. Lyon, G.R. Dejong, *Theory and Application of Statistical Energy Analysis*, Butterworth-Heinemann, Boston, 1995.
[2] J.C. Wohlever, R.J. Bernhard, Mechanical energy flow models of rods and beams, *Journal of Sound and Vibration* 153 (1992) 1–19.
[3] P.E. Cho, R.J. Bernhard, Energy flow analysis of coupled beams, *Journal of Sound and Vibration* 211 (1998) 593–605.
[4] O.M. Bouthier, R.J. Bernhard, Simple models of the energy flow in vibrating membranes, *Journal of Sound and Vibration* 182 (1995) 129–147.
[5] O.M. Bouthier, R.J. Bernhard, Simple models of the energetics of transversely vibrating plates, *Journal of Sound and Vibration* 182 (1995) 149–166.
[6] F. Bitsie, R.J. Bernhard, Sensitivity calculations for structural-acoustic EFEM predictions, *Noise Control Engineering* 46 (1998) 91–96.

[7] J.F. Doyle, *Wave Propagation in Structures: Spectral Analysis Using Fast Discrete Fourier Transforms*, second ed., Springer, New York, 1997.
[8] E.R.O. Santos, High Frequency Vibration Analysis by Energy Methods, PhD Thesis, State University of Campinas—UNICAMP, 2006.
[9] J. Plunt, C. Fredo, M. Sanderson, On the use and misuse of the statistical energy analysis for vehicle noise control, *Proceedings of the SAE Noise and Vibration Conference*, Michigan, USA, 1993, pp. 319–328.
[10] K.M. Ahmida, J.R.F. Arruda, Exact modeling of kinetic energy in truss-type members, *Journal of Sound and Vibration* 267 (2003) 167–177.
[11] L. Cremer, M. Heckl, *Structure-Borne Sound: Structural Vibrations and Sound Radiation at Frequencies*, second ed., Springer, Berlin, 1988.
[12] I. Moens, D. Vandepitte, P. Sas, Study of the applicability of the energy finite element method for plates, *NOVEM International Conference*, Lyon, France, 2000, pp. 1–12.